PHYSICAL REVIEW B VOLUME 26, NUMBER 8 15 OCTOBER 1982

Phonon density-of-states effect in resonant neutron interferometry: Theory and measurement for isotopically pure ^{149}Sm

R. E. Word and S. A. Werner
Physics Department, University of Missouri, Columbia, Missouri 65211
(Received 23 February 1982)

Neutron interferometry furnishes a means of measuring directly the coherent part of the forward-scattering amplitude. We report here a measurement of the low-lying thermal resonance in isotopically pure ^{149}Sm, which enables the determination of the Breit-Wigner resonant parameters. Statistically significant deviations from the Breit-Wigner resonant line shape are seen. These deviations are interpreted in terms of phonon contributions to the Doppler-shift-modified line shape, which in a leading-order asymptotic approximation involves an effective temperature parameter T_{eff} for metallic samarium, just as in the case of Doppler-broadened resonant absorption.

I. INTRODUCTION

Near a resonance, the neutron scattering amplitude exhibits a dependence on the incident energy of the neutron that is given by the Breit-Wigner formula[1]; the magnitude of the resonant contribution to the scattering amplitude is Lorentzian, while the phase of this contribution goes from zero to π through the resonance. Neutron transmission experiments provide a means of measuring the neutron absorption cross section, which by the optical theorem in quantum mechanics is proportional to the imaginary part of the forward scattering amplitude. Studies of anomalous neutron diffraction from samples containing a resonantly scattering isotope[2–6] enable the phase variation to be seen; since the static structure factor itself has differing contributions in phase from the different species of atomic constituents in the sample crystal at various Bragg angles, the phase variation of the resonantly scattering constituent may be obtained with the use of standard crystallographic techniques. However, this method involves averaging over many different Bragg scattering angles in the crystallographic fit, which may mask the presence of an angular variation in the resonant scattering amplitude.

Neutron interferometry furnishes a means of obtaining directly the real and imaginary parts of the scattering amplitude in the single direction of forward scattering; the wave function of the neutron undergoes a phase shift in consequence of passage through a sample that is proportional to the real part of the forward scattering amplitude, while the magnitude of the wave function is diminished in a ratio proportional to the imaginary part of the forward coherent scattering amplitude. This method allows the study of a sample with a single species of atomic constituent. We report here an interferometric measurement of the real part of the forward scattering amplitude in isotopically pure ^{149}Sm metal at a variety of incident wavelengths close to a Breit-Wigner resonance. However, our data indicate deviations from a strict Breit-Wigner resonant line shape.

Bethe and Placzek[7] first showed that nuclear resonances are modified by the motions of the target nuclei; resonant absorption of neutrons by nuclei bound in crystals was considered by Lamb,[8] who showed how the presence of phonon modes in the target crystal would modify the resonant absorption curve. Resonant diffraction was investigated by Trammell,[9] who developed the resonant scattering amplitude in a correlation-function formalism in order to compute the elastic scattering at resonance from bound nuclei. It is the long "delay time" $\hbar/\Gamma$ (where Γ is the width of the resonance) between the entrance and emergence of the neutron from the nucleus in resonant (n,n) scattering that enables the nucleus to probe its environment during the scattering process, thus giving rise to condensed-matter modifications to the Breit-Wigner resonant line shape. As we shall show, these modifications are largest in the direction of forward scattering, which is observed in neutron interferometry. In the next section, we shall compute the deviations from the Breit-Wigner resonance associated with the phonon

density of states in metallic samarium, and then we shall show in the description of the experimental results that these deviations are of the same magnitude as those seen in the interferometric measurement.

II. AN EVALUATION OF THE RESONANT SCATTERING AMPLITUDE FOR ^{149}Sm IN DISPERSION THEORY

In the vicinity of a resonance the (n,n) scattering amplitude for a free nucleus at rest may be written

$$f=f_0+f_R \ , \tag{2.1}$$

where f_0 is the potential scattering amplitude and f_R is the resonant (n,n) scattering amplitude, which is expressed by the Breit-Wigner formula when the motions of the target nuclei may be neglected:

$$f_R=\lambda\!\!\!^{-}g\mu\frac{\Gamma_n}{E-E_R-R-i\Gamma/2} \ . \tag{2.2}$$

In (2.2), $\lambda\!\!\!^{-}$ is the wavelength of the incident neutron over 2π, g is a factor for the spin multiplicity given by

$$g=\frac{j+\frac{1}{2}}{2I+1} \ , \tag{2.3}$$

where j is the spin of the resonant channel and I is the spin of the nuclear ground state. E is the energy of the incident neutron, E_R is the energy of the center of the resonance, R is the recoil energy

$$R=(m/M)E \tag{2.4}$$

(where m is the mass of the neutron and M is the mass of the target nucleus), μ is the reduced mass of the neutron and target nucleus, Γ is the total width of the resonance, and Γ_n is the neutron partial width. In ^{149}Sm a low-lying thermal resonance occurs at $E_R=0.096$ eV with a total width of $\Gamma=0.065$ eV and a neutron partial width of $\Gamma_n=0.000\,56$ eV; the resonance occurs in the $j=I+\frac{1}{2}$ channel, where $I=\frac{7}{2}$.[10] This resonance is accessible to thermal neutrons from a reactor source.

The motions of the target nuclei will modify the Breit-Wigner line shape so that in the single collision approximation[11] the coherent resonant scattering amplitude may be expressed in terms of two-time correlation functions[9,12]:

$$f_R(\vec{k}_0,\vec{k}_f)=(\Gamma_n/2i\hbar k_0)g\mu \times\int_0^\infty dt\exp\left[\frac{i}{\hbar}\Delta Et\right] \times\langle e^{-i\vec{k}_f\cdot\vec{r}(t)}e^{i\vec{k}_0\cdot\vec{r}(0)}\rangle \ , \tag{2.5}$$

where $\vec{k}_0$ and $\vec{k}_f$ are the incident and final-state wave vectors of the neutron, respectively, $\Delta E=E-(E_R+i\Gamma/2)$, and $\vec{r}(t)$ is the position operator of the target neucleus in the Heisenberg representation [so that (2.5) is the resonant scattering amplitude per target nucleus]. Thus in general, the coherent resonant scattering amplitude exhibits an angular dependence which is bound up with an interaction between the scattering and condensed-matter Hamiltonian.

The expression (2.5) is given asymptotically to leading order in the parameter ΔE by (2.2):

$$f_R(k_0,k_f)\sim e^{-2W(\Delta\vec{k})}(\Gamma_n g\mu/2k_0)/\Delta E \ , \tag{2.6}$$

where $\Delta\vec{k}$ is the momentum transfer to the neutron upon scattering and $W(\Delta\vec{k})$ is the usual Debye-Waller factor. Thus the coherent resonant scattering amplitude satisfies the sum rule[12]

$$\int_{-\infty}^{\infty}dE\,f_R(\Delta\xi,\Delta\vec{k},\Delta,\phi_k) =i\pi e^{-2W(\Delta\vec{k})}(\Gamma_n g\mu/2k_0) \ , \tag{2.7}$$

where $\Delta\xi$ is the energy transfer to the neutron upon scattering, $\Delta=E-E_R$, ϕ_k is the azimuthal angle of the k_0k_f plane (i.e., the plane of the scattering triangle) about the axis $\Delta\vec{k}$, and the integral is to be performed by varying Δ while leaving the remaining arguments constant. In the case of neutron interferometry $\vec{k}_0=\vec{k}_f$, so that the Debye-Waller factor in (2.6) and (2.7) goes to unity. Hence (2.7) shows that condensed-matter processes merely redistribute scattering amplitude without changing its total area; the total area under the real part of the scattering amplitude is zero by (2.7). It should be pointed out that Γ_n exhibits a $\sqrt{E}$ variation, so that the last factor on the right-hand side of (2.7) may be given its value at $E=E_R$.

The correlation function on the right-hand side of (2.5) may be evaluated in the harmonic approximation by using Bloch's formula; one obtains

$$\langle e^{-i\vec{k}_f\cdot\vec{r}_i(t)}e^{i\vec{k}_0\cdot\vec{r}_i(0)}\rangle=\exp(-\tfrac{1}{2}\{\langle(\vec{k}_0\cdot\vec{r}_i)^2\rangle+\langle(\vec{k}_f\cdot r_i)^2\rangle+2\langle[\vec{k}_f\cdot\vec{r}_i(t)][\vec{k}_0\cdot\vec{r}_i(0)]\rangle\}) , \tag{2.8}$$

where i indexes the scattering site. The position operators in terms of the usual Bose operators may be written

$$\vec{r}_{\vec{i},\alpha}(t)=\sum_{j,\vec{q}}\left[\frac{\hbar}{2NM\omega_j(\vec{q})}\right]^{1/2}\{\vec{\sigma}_\alpha^j(\vec{q})\exp[i\vec{q}\cdot\vec{i}-i\omega_j(\vec{q})t]a_j(\vec{q}) + \vec{\sigma}_\alpha^{j*}(\vec{q})\exp[-i\vec{q}\cdot\vec{i}+i\omega_j(\vec{q})t]a_j^\dagger(\vec{q})\} , \tag{2.9}$$

where $\vec{i}$ indexes the lattice site, α indexes an occupied site in the unit cell, j refers to the phonon mode in question, N is the total number of unit cells in the sample, $\omega_j(\vec{q})$ is the angular frequency of the jth phonon mode of wave vector $\vec{q}$, M is the mass of the samarium nucleus, the σ's refer to the phonon eigenvectors, which satisfy the orthonormality relation

$$\sum_\alpha\vec{\sigma}_\alpha^{j*}(\vec{q})\cdot\vec{\sigma}_\alpha^{j'}(\vec{q})=\delta_{j,j'} , \tag{2.10}$$

and the a's are the Bose operators. Using (2.9), one may write the correlation function in terms of the phonon density of states:

$$\langle[\vec{k}_f\cdot\vec{r}_i(t)][\vec{k}_0\cdot\vec{r}_i(0)]\rangle=\frac{3\hbar}{2M}k_0k_f\int_{-\infty}^{\infty}d\omega\,[n(\omega)+1]\frac{Z(\omega)}{\omega}\langle(\hat{k}_f\cdot\vec{\sigma}^*)(\hat{k}_0\cdot\vec{\sigma})\rangle_{\rm av}\exp(-i\omega t) . \tag{2.11}$$

The left-hand side of (2.11) is an average over the various symmetry sites occupied by the samarium nucleus in the unit cell; $n(\omega)$ is the phonon occupation number of a phonon mode of angular freqency ω, which is given by

$$n(\omega)=\frac{e^{-\beta\omega}}{1-e^{-\beta\omega}} \tag{2.12}$$

(where β is the inverse temperature in units of time), $Z(\omega)$ is the normalized density of phonon states

$$Z(\omega)=\frac{1}{3N}\sum_{j,\vec{q}}[\delta(\omega-\omega_j(\vec{q}))+\delta(\omega+\omega_j(\vec{q}))] , \tag{2.13}$$

$\hat{k}_f$ and $\hat{k}_0$ are unit vectors in the direction of $\vec{k}_f$ and $\vec{k}_0$, respectively. The last factor on the right-hand side of (2.11) is given by

$$\langle(\hat{k}_f\cdot\hat{\sigma}^*)(\hat{k}_0\cdot\vec{\sigma})\rangle_{\rm av}=\sum_{j,\alpha}\left[\int d\Omega_q[\hat{k}_f\cdot\vec{\sigma}_\alpha^{j*}(\vec{q})][\hat{k}_0\cdot\vec{\sigma}_\alpha^j(q)]\right]\Big/\left[\int d\Omega_q\right]\ [\omega<\omega_j(\vec{q})<\omega+d\omega] , \tag{2.14}$$

where the integral is evaluated in $\vec{q}$, subject to the indicated restraint. Taking components of the eigenvectors, the dyadic

$$A^{\mu\nu}(\omega)=\sum_{j,\alpha}\left[\int d\Omega_q\sigma_\alpha^{j(\mu)*}(\vec{q})\sigma_\alpha^{j(\nu)}(\vec{q})\right]\Big/\left[\int d\Omega_q\right]\ [\omega<\omega_j(\vec{q})<\omega+d\omega] \tag{2.15}$$

is a Hermitian matrix, and therefore it must have real eigenvalues. The crystal structure of metallic samarium is rhombohedral (space group $R\bar{3}m$) with three atoms per unit cell[13,14] (and hence the inclusion of optic phonon modes in the above formalism). Figure 1 shows the crystal structure of metallic samarium. By virtue of the trigonal symmetry (2.15) can have no nonvanishing elements between directions normal and parallel to the trigonal axis, respectively; since the eigenvectors of (2.15) must be normal, the dyadic A must have a doubly degenerate eigenvalue with associated eigenvectors spanning the plane normal to the trigonal axis. Therefore, letting ι (ρ) be the value of (2.14) when $\vec{k}_0=\vec{k}_f$ and $\vec{k}_0$ is normal to (parallel to) the trigonal axis, the average (2.14) may be written more generally as follows:

$$\langle(\hat{k}_f\cdot\vec{\sigma}^*)(\hat{k}_0\cdot\vec{\sigma})\rangle_{\rm av}=\rho\cos(\theta_0)\cos(\theta_f)+\iota\sin(\theta_0)\sin(\theta_f) , \tag{2.16}$$

where θ_0 and θ_f are the angles of $\vec{k}_0$ and $\vec{k}_f$ with respect to the trigonal axis in metallic samarium. For the sake of simplicity in the following discussion, we shall set $\vec{k}_0$ to be parallel to the trigonal axis. Then substituting (2.11) and (2.8) and (2.5), the coherent resonant scattering amplitude with the inclusion of the phonon modifications can be written

$$f_r(\vec{k}_0,\vec{k}_f)=(\Gamma_n/2\hbar k_0)g\mu e^{-[W(\vec{k}_0)+W(\vec{k}_f)]}\left[\frac{\hbar}{\Delta E}+\sum_{n=1}^{\infty}\frac{\chi^n}{n!}\int_{-\infty}^{\infty}d\omega\frac{p_n(\omega)}{(\Delta E/\hbar)-\omega}\right], \tag{2.17}$$

where the expansion parameter is

$$\chi=\frac{3\hbar}{2M}k_0k_f\cos(\theta_f) \tag{2.18}$$

and the p's are a series of successively convoluted functions defined such that

$$p_1(\omega)=\rho[n(\omega)+1]\frac{Z(\omega)}{\omega} \tag{2.19}$$

and

$$p_{n+1}(\omega)=\int_{-\infty}^{\infty}d\omega' p_1(\omega')p_n(\omega-\omega') . \tag{2.20}$$

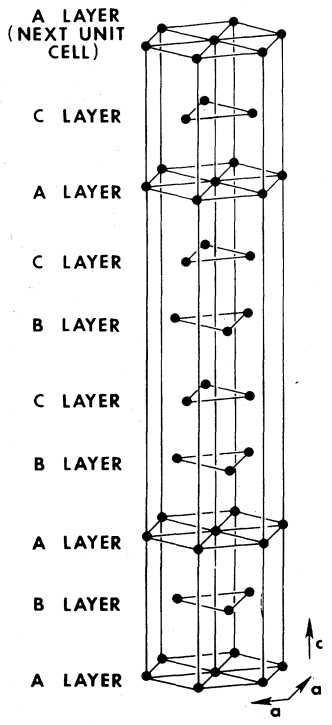

FIG. 1. Crystal structure of metallic samarium. Metallic samarium satisfies $R3m$ symmetry with three atoms per rhombohedral unit cell. However, the structure can be viewed as a nine-layer close-packed hexagonal layer scheme as depicted above; the nine layers span about 9 Å.

The formula (2.17) is an exact expansion for the coherent scattering amplitude in the harmonic approximation. It should be noted that the leading-order term in χ exhibits an angular variation proportional to $\cos(\theta_f)$, so that the phonon density-of-states modification to the resonant line shape largely disappears if an angular average is performed. The advantage of looking for these effects via neutron interferometry is that they are largest in the direction of forward scattering; there is no danger of losing these contributions by averaging over many different Bragg angles, which may occur in diffraction studies.

Figure 2 is a plot of the real part of (2.17) computed to second order in χ for a Debye model of samarium. The Debye temperature of metallic samarium is about 169 K (Ref. 15); treating the acoustic modes isotropically, we may set $\rho\simeq\frac{1}{3}$, and the phonon density of states becomes

$$Z(\omega)=3\frac{\omega^3}{\omega_D^3}, \quad |\omega|<\omega_D$$
$$Z(\omega)=0, \quad |\omega|>\omega_D \tag{2.21}$$

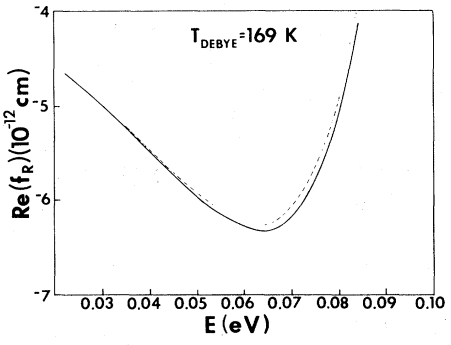

FIG. 2. Computation of the resonant forward scattering amplitude in the Debye model. Incident neutron energies in eV are plotted on the horizontal axis; scattering amplitudes in units of cm are plotted on the vertical axis. The solid line is the real part of the unmodified resonant scattering amplitude for ^{149}Sm as given by (2.2); the broken line is the quantity (2.17) computed to second order in the forward scattering direction ignoring anisotropies and with the use of Debye temperature of 169 K.

where ω_D is the Debye frequency. Hence, it is found that the acoustic modes should give rise to about a 1% modification of the real part of the resonant scattering amplitude in the region of interest. However, as Lamb showed long ago,[8] the zero-point motions associated with the optic modes can give rise to a large contribution even when these modes are not excited at the temperature of the experiment. Therefore, we compute the scattering amplitude in the weak-binding approximation, which is valid when $\Gamma/2 \gg k\Theta_D$, which is true of metallic samarium, which includes the effects of the optical modes in an effective temperature.

The series (2.17) does not satisfy the sum rule (2.7) term by term because of the variation of the Debye-Waller factor with incident wave vector (a condition that is associated with its nonuniform convergence); thus in some instances its leading-order terms may give rise to an erroneous impression of the nature of the redistribution of scattering amplitude arising from the presence of the phonon modes. On the other hand, the leading-order terms in the weak-binding approximation satisfy the requisite sum rule automatically. In order to obtain the latter approximation, we write

$$\vec{r}(t)=\vec{r}(0)+t\frac{\vec{p}}{M}+\cdots , \tag{2.22}$$

where $\vec{p}$ is the momentum operator for the target nucleus at $t=0$. Substituting (2.22) into (2.5), and using once again the Bloch formula which is valid in the harmonic approximation, one obtains

$$f_R(\vec{k}_0,\vec{k}_0)=(\Gamma_n/2i\hbar k_0)g\mu\int_0^\infty dt\, e^{(i/\hbar)\Delta E' t}\exp\left[-\frac{k_0^2}{2M}\left\langle\frac{p^2}{M}\right\rangle t^2\right]$$

$$=(\Gamma_n/2i\hbar k_0)g\mu\exp\left[-\left[\frac{\Delta E'}{\hbar}\right]^2\Big/\left[4\frac{k_0^2}{2M}\left\langle\frac{p^2}{M}\right\rangle\right]\right]\operatorname{erfn}\left[i\frac{\Delta E'}{\hbar}\Big/2\left[\frac{k_0^2}{2M}\left\langle\frac{p^2}{M}\right\rangle\right]^{1/2}\right] . \tag{2.23}$$

The derivation of (2.23) involves a commutator between position and momentum, which has required the redefinition of the resonant parameter to

$$\Delta E'=\Delta E+\frac{\hbar^2k_0^2}{2M} , \tag{2.24}$$

which is essentially the effect of recoil. The function on the right-hand side of (2.23) has an asymptotic development that may be written

$$\exp\left[-\frac{A^2}{4B}\right]\operatorname{erfn}\left[i\frac{A}{2\sqrt{B}}\right]\sim\frac{i}{A}\sum_{n=0}^{\infty}\left[-\frac{B}{A^2}\right]^n\frac{(2n)!}{n!}$$

so that the right-hand side of (2.23) to leading order in $1/\Delta E'^2$ is given by

$$f_R(\vec{k}_0,\vec{k}_0)\sim(\Gamma_n/2\hbar k_0)\times g\mu\left[\frac{1}{\Delta E'}-\frac{2(k_0^2/2M)(\langle p^2/M\rangle)}{\Delta E'^3/\hbar^2}\right] . \tag{2.25}$$

The second term in (2.25) is the correct form of the asymptotic coefficient bearing an exact relation to the resonant line shape, which has been obtained elsewhere[12] with the neglect of the force density contribution (hence the "weak-binding approximation"). The momentum-squared correlation function is given in terms of the Bose occupation by

$$\langle p^2/M\rangle=\kappa T_{\text{eff}}=\sum_{\vec{q},j}\hbar\omega_j(\vec{q})\{n[\omega_j(\vec{q})]+\tfrac{1}{2}\}/N , \tag{2.26}$$

where T_{eff} is an effective temperature parameter; the term $\frac{1}{2}$ on the right-hand side of (2.26) expresses the contribution that arises from zero-point motion. Since samarium metal has three atoms per unit cell, its lattice dynamics will contain

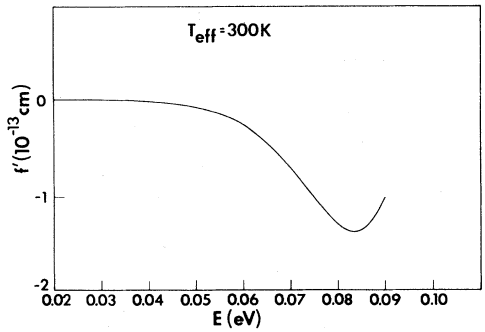

FIG. 3. Plot of the leading-order modification to the resonant line shape in the model of (2.27). Incident neutron energies are plotted on the horizontal axis, while the real part of the leading-order modification to the resonant line shape is plotted on the vertical axis. For this computation T_{eff} is set equal to room temperature.

six optic-phonon modes in addition to the three acoustic modes; optic modes typically can cause T_{eff} to be much larger than room temperature through the mechanism of zero-point motion. Figure 3 is a plot of the real part of the second term in (2.25) when T_{eff} is room temperature; it is seen to give rise to an enhancement of the resonance minimum in the energy region of interest.

By substituting (2.26) into (2.25), the (n,n) scattering amplitude (2.1) can be written to leading orders

$$f_R(\vec{k}_0,\vec{k}_0)=f_0+\frac{\Gamma_n}{2\hbar k_0}\frac{g\mu}{\Delta E'}\left[1-2\left[\frac{m}{M}\right]\frac{E\kappa T_{\text{eff}}}{\Delta E'^2}\right]. \tag{2.27}$$

Since the modifications to the resonant line shape are expected to be no more than a few percent, the leading-order asymptotic expansion (2.27) should suffice for its description. Although in principle the resonant line shape contains the more detailed density-of-states information (2.19), in using (2.27) to fit the interferometric measurement described in the next section, we shall obtain the parameter T_{eff}, which involves an integral over the density of states (2.26). The coefficients of an asymptotic expansion for a given function do not contain the complete information about a function; in this case the determination of more detailed information about the phonon density of states in metallic samarium by interferometric means would require measurements over a more extensive region of energy than has proved possible on a reactor source.

III. DESCRIPTION OF THE EXPERIMENTAL PROCEDURE AND RESULTS

Neutron interferometry furnishes a means of obtaining directly the real and imaginary parts of the coherent scattering amplitude; the phase shift $\Delta\phi$ experienced by the neutron wave function in consequence of passage through a sample of atomic density n and uniform thickness t is given by

$$\Delta\phi=\text{Re}(nft\lambda)\,, \tag{3.1}$$

while the magnitude of the amplitude of the neutron wave is diminished through the ratio

$$r=\exp[-\text{Im}(nft\lambda)]\,, \tag{3.2}$$

where λ is the wavelength of the neutron. We report here an interferometric measurement of the real part of the coherent scattering length in isotopically pure ^{149}Sm at a variety of incident wavelengths over which the scattering amplitude is rapidly changing due to the presence of a low-lying thermal resonance.

The experiment described here was carried out at the 10-MW University of Missouri Research Reactor on Beam Port B; a pyrolitic graphite double-crystal monochromator prepared the incident beam with a wavelength resolution of about 1%. A highly perfect silicon crystal, which was cut in the form of a Bonse-Hart interferometer of the symmetric type,[16,17] provided the means of splitting the incident beam coherently along two different paths separated by a distance of the order of a few centimeters. Figure 4 illustrates the geometry of the interferometer. A stepping motor enabled a mounted sample to be driven in and out of the path of the incident neutron, corresponding to one of the two widely separated paths taken simultaneously by the neutron. A slab of silicon or aluminum of thickness T that could be rotated freely was put in the second leg of the interferometer and it served as a "phase flag" by which the relative phase, or optical path length, of the two widely separated paths could be determined. A ^{3}He detector mounted at an adjustable position centered on the relevant exiting beam as shown in Fig. 4 served to measure the intensity arising from the interference of the two coherent waves.

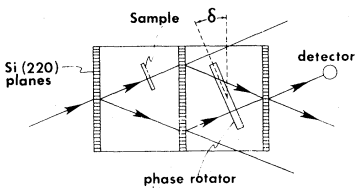

FIG. 4. Geometry of the interferometer. The sample is driven in and out of one of the two coherent paths taken by the neutron while the phase rotator varies in angle of orientation in discrete steps. The detector is centered on the Bragg reflection.

If δ is the angle made by the vertical rotator strip relative to the blades of the interferometer, then by (3.1) the phase difference introduced by the rotator between the two coherent paths may be shown to be

$$\beta_{\text{rot}}=-2\lambda\nu b_{\text{rot}}T\frac{\sin(\delta)\sin(\theta_B)}{\cos^2(\theta_B)-\sin^2(\delta)}\,, \tag{3.3}$$

where θ_B is the Bragg angle of the interferometer crystal, b_{rot} is the real part of the coherent forward scattering amplitude of the rotator, and ν is the atomic density of the latter. Thus the intensity measured by the ^{3}He detector exhibits oscillations as a function of the angular expression in δ in (3.3),

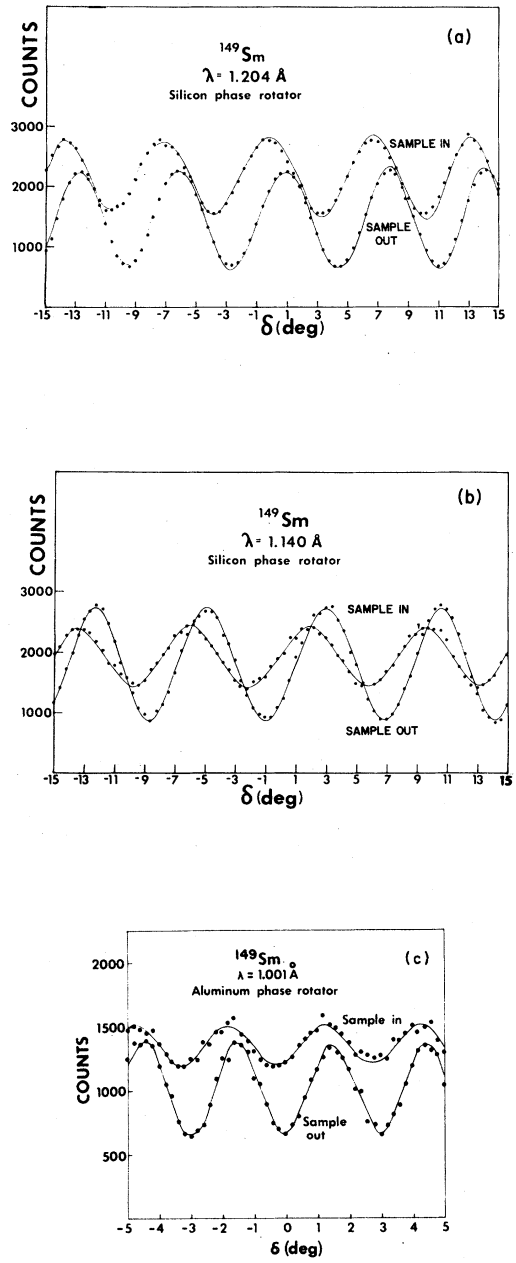

FIG. 5. Sample raw-data sets from the interferometric measurement. (a) Data taken at a wavelength of 1.204 Å with the use of the silicon phase rotator. The upper curve is for sample in, which was obtained by counting for 186 s; the lower curve is for sample out, with a counting time of 71.6 s. (b) Data taken at a wavelength of 1.140 Å; the sample in counting time was 203 s per point, while the sample out counting time was 163 s. (c) Data taken at 1.001 Å; the upper curve for sample in was counted for 506 s per point, while the lower curve was counted for 208 s. The diminution in the amplitude of the sample in curve is due to absorption in the sample.

the period of which varies inversely as λ. Thus the period of the sinusoidal wave determines λ (since the Bragg angle of the interferometer also depends on λ, it is necessary to use an iterative procedure in the data analysis). Repeating a given run a number of times in order to reduce the statistical error, our experiment yielded values for λ typically good to about one part in 10^4. The thickness of the silicon phase rotator was 0.2931 cm, while the aluminum phase rotator was of thickness 1.012 cm.

The ^{149}Sm sample used in the experiment was a thin foil of thickness $t = 10.27$ μm obtained from the Isotope Division, of the Oak Ridge National Laboratory. This thickness was chosen as a compromise between excessive absorption attenuation and a measurable phase shift. The sample was driven in and out of the first path taken by the neutron in the interferometer as δ was varied in a discrete and regular fashion point by point. Thus two sinusoidal curves were obtained for each run, one giving the number of neutrons counted by the ^{3}He detector when the sample was out of the path for a range of rotator angles, and a second giving the neutron counts (for some second time interval at each point) for the same range. The difference in phase of the two sinusoids constituted a measurement of the quantity $\Delta\phi$ in (3.1), the phase shift introduced by the presence of the sample. The data were analyzed by fitting it to a cosine function of the angular argument in (3.3) utilizing a linear least-squares multivariate regression program. The error bars were obtained by repeating the measurement at a given wavelength several times.

The data reported here were taken with the use of the (220) reflection on the silicon interferometer, and the (004) and (006) reflections of the graphite double-crystal monochromator at, respectively, longer and shorter wavelengths. Figure 5 shows some typical data taken at three different incident wavelengths, respectively. Figures 5(a) and 5(b) depict data taken utilizing the (004) graphite reflection for which the silicon rotator was employed. Figure 5(c) shows data taken utilizing the (006) graphite reflection for which a thick aluminum rotator was employed in order to obtain more sinusoidal periods within the angular range of δ, which was required at the shorter wavelengths. The latter figure shows a marked decline in the contrast for the sample in data, which arises from the loss of intensity in the sample path associated with absorption, as given by (3.2).

Table I shows the measured phase shifts and associated real coherent scattering lengths for the

TABLE I. Tabulation of incident neutron wavelength versus the measured real part of the forward scattering amplitude in ^{149}Sm.

λ (Å)	E (eV)	Re(f) (10^{-12} cm)
1.6725	0.029 45	1.87±0.028
1.6725	0.029 45	1.85±0.13
1.605	0.031 98	2.03±0.12
1.557	0.033 96	2.117±0.018
1.556	0.034 01	2.123±0.034
1.555	0.034 08	2.16±0.021
1.502	0.036 50	2.09±0.049
1.451	0.039 13	2.00±0.038
1.451	0.039 13	1.97±0.041
1.403	0.041 85	2.194±0.02
1.398	0.0421	2.35±0.07
1.296	0.049 04	2.38±0.05
1.284	0.049 93	2.44±0.043
1.269	0.051 15	2.48±0.04
1.266	0.051 39	2.4 ±0.05
1.257	0.052 11	2.63±0.029
1.257	0.052 11	2.62±0.03
1.210	0.056 25	2.81±0.07
1.204	0.056 85	2.82±0.027
1.178	0.059 36	2.77±0.023
1.167	0.060 48	2.92±0.057
1.153	0.061 96	3.00±0.057
1.140	0.063 39	2.84±0.054
1.090	0.069 37	2.63±0.032
1.036	0.076 69	2.35±0.067
1.023	0.078 65	2.44±0.054
1.001	0.081 32	1.637±0.10
0.9676	0.087 98	1.295±0.038
0.9424	0.092 74	1.00±0.22

^{149}Sm sample at a variety of incident energies ranging from 0.029 to 0.093 eV; Fig. 6 is a graphical representation of these numbers. The resonant parameters may be obtained by fitting five points on the steep slope near the center of the resonance to (2.2), for which $\Delta\phi$ varies greatly while E varies slightly. Then one obtains $E_R \simeq 0.096$ eV and $\Gamma \simeq 0.064$ eV, which is in good agreement with the accepted values.

Near the center of the minimum of the real part of the scattering length, the interferometric data reveals systematically a discrepancy of the order 4% from the Breit-Wigner variation; hence we fit the data against (2.27) in order to account for dispersion in the sample. The solid line in Fig. 6 is the best fit to the data from which one finds the following values of the potential scattering amplitude (in cm) for ^{149}Sm and the effective temperature (at room temperature in K) for metallic samarium:

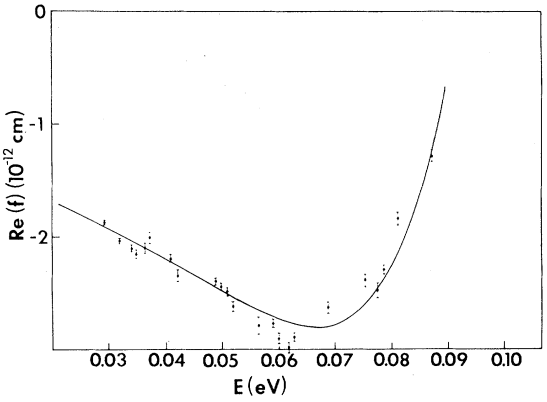

FIG. 6. Plot of the real part of the forward scattering amplitude for ^{149}Sm as measured in the interferometry experiment. The points develop a systematic enhancement of several percent between 0.05 and 0.06 eV beyond that given by the Breit-Wigner variation. The solid curve is the best fit of the model (2.27) to the data, which requires an effective temperature of 735 K, and a potential scattering amplitude of 0.88×10^{-12} cm.

$$f_0=(0.84\pm0.027)\times10^{-12}\ ,$$

$$T_{\rm eff}=735\pm241)\ .$$

However, the interpretation of the data in terms of the model (2.27) is somewhat ambiguous for the following reasons: (a) The uncertainty in the solid-state parameter $T_{\rm eff}$ given by the multivariate regression of the data in terms of the requisite model is large; (b) The minimum in the experimental data is displaced in energy somewhat from that which would be given by the model (2.27). Hence the interpretation of the observed deviations from the Breit-Wigner variation (which are statistically significant) as a solid-state effect in the model (2.27) is tentative.

IV. CONCLUSION

We have performed an interferometric measurement of the real part of the coherent (n,n) forward scattering amplitude in ^{149}Sm for a variety of incident wavelengths over which a low-lying thermal resonance is developed. The measurement indicates a deviation at the 4% level from the strict Breit-Wigner resonance line shape, which can be accounted for by the coupling in dispersion theory to the phonon density of states of the resonant scattering. We have determined the potential scattering amplitude for ^{149}Sm and the value of the effective temperature parameter $T_{\rm eff}$ at room temperature for metallic samarium.

Anomalous dispersion is a means that has been used to solve the phase problem in neutron crystallography.[2–6] Since this previous work typically has not accounted for dispersion in the sample, our result suggests that it may contain systematic errors.

ACKNOWLEDGMENTS

The authors wish to thank G. T. Trammell, G. Alldredge, T. Wolfram, and others for conversations on this and related topics. We wish to express our gratitude to the following members of the Missouri University Research Reactor (MURR) staff for the helpfulness which they showed: R. Berliner, D. Mildner, W. Yelon, and F. Ross. Special thanks are extended to Professor Chandrasekhar and Professor Hensley for their help in polishing the silicon and aluminum phase rotators used in this experiment. The advice and expertise of C. Holmes and S. Potts of the machine shop are greatly appreciated. This work was supported by NSF Grant No. PHY-79-20979.

[1]G. Breit and E. Wigner, Phys. Rev. 49, 519 (1936).
[2]S. W. Peterson and H. G. Smith, Phys. Rev. Lett. 6, 7 (1961).
[3]H. G. Smith and S. W. Peterson, J. Phys. (Paris) 25, 615 (1964).
[4]Richard J. Flook, Hans C. Freeman, and Marcia L. Scudder, Acta Crystallogr. Sect. B 33, 801 (1977).
[5]H. D. Bartnik, Acata Crystallogr. Sect. A 34, 747 (1978).
[6]D. W. Engel and T. F. Koetzle, in *Proceedings of the 1981 Neutron Scattering Symposium, Argonne, 1981,* edited by J. Faber (American Institute of Physics, New York, 1982).
[7]H. A. Bethe and G. Placzek, Phys. Rev. 51, 462 (1937).
[8]W. E. Lamb, Phys. Rev. 55, 190 (1939).
[9]G. T. Trammell, Phys. Rev. 126, 1046 (1962).
[10]D. J. Hughes and R. Schwartz, *Neutron Cross Sections* (U.S. GPO, Washington, D.C., 1958).
[11]G. T. Trammell and J. D. Chalk, Phys. Rev. 141, 815 (1966).
[12]R. E. Word and G. T. Trammell, Phys. Rev. B 24, 2430 (1981).
[13]A. H. Daane, R. E. Rundle, H. G. Smith, and F. H. Spedding, Acta. Crystallogr. 7, 532 (1954).
[14]W. C. Koehler and R. M. Moon, Phys. Rev. Lett. 29, 1468 (1972).
[15]M. Rosen, Phys. Rev. 180, 540 (1969).
[16]U. Bonse, *Neutron Interferometry* (Clarendon, Oxford, 1979).
[17]J.-L. Staudenmann, S. A. Werner and R. Colella, Phys. Rev. A 21, 1419 (1980).